POLITECNICO DI TORINO
Repository ISTITUZIONALE

Real-time monitoring of fat crystallization using pulsed acoustic spectroscopy and supervised machine learning

Original
Real-time monitoring of fat crystallization using pulsed acoustic spectroscopy and supervised machine learning / Metilli, L.; Morris, L.; Lazidis, A.; Marty-Terrade, S.; Holmes, M.; Povey, M.; Simone, E.. - In: JOURNAL OF FOOD ENGINEERING. - ISSN 0260-8774. - ELETTRONICO. - 335:(2022), p. 111192. [10.1016/j.jfoodeng.2022.111192]

Availability:
This version is available at: 11583/2969868 since: 2022-07-07T19:30:33Z

Publisher:
Elsevier Ltd

Published
DOI:10.1016/j.jfoodeng.2022.111192

Terms of use:

This article is made available under terms and conditions as specified in the corresponding bibliographic description in the repository

Publisher copyright
Elsevier postprint/Author's Accepted Manuscript

© 2022. This manuscript version is made available under the CC-BY-NC-ND 4.0 license http://creativecommons.org/licenses/by-nc-nd/4.0/.The final authenticated version is available online at: http://dx.doi.org/10.1016/j.jfoodeng.2022.111192

(Article begins on next page)

25 April 2024

Real-time monitoring of fat crystallization using pulsed acoustic spectroscopy and supervised machine learning

Lorenzo Metilli[1], Liam Morris[1], Aris Lazidis[2], Stephanie Marty-Terrade[3], Melvin Holmes[1], Megan Povey[1] and Elena Simone[1,4]

[1] School of Food Science and Nutrition, Food Colloids and Bioprocessing group, University of Leeds, Woodhouse Lane, Leeds LS2 9JT, UK

[2] Nestlé Product Technology Centre Confectionery, Haxby Road, York YO31 8TA, UK

[3]Nestlé Research, Vers-chez-les-Blanc, 1000 Lausanne 26, Switzerland

[4] Department of Applied Science and Technology (DISAT), Politecnico di Torino, Torino (Italy)

KEYWORDS

Crystallization, Fats, Oils, Ultrasound, Machine Learning

ABSTRACT

Enhancing the control and yield of lipid crystallization is fundamental in several industrial areas, including pharmaceutical, cosmetic and food manufacturing. However, the multi-component nature of fats and oils poses a challenge in the understanding and control of the final product properties. While the crystallization of lipid has been extensively studied with offline techniques, online monitoring of the process would be highly advantageous, especially in large-scale sheared vessels. In this work, a novel method to calculate the solid fat content (SFC%) of crystallizing lipids under shear, based on an acoustic probe and supervised-machine learning, is presented. The temperature, composition and ultrasonic velocity of the samples, and the SFC(%) measured with nuclear magnetic resonance were used to develop a predictive model to calculate the SFC(%) during crystallization. Gaussian models showed the highest accuracy compared to linear and regression tree models (RMSE = 0.03 vs 0.7 and 0.25, respectively).

1. Introduction

The crystallization of lipids is a fundamental unit operation for several manufacturing industries, including pharmaceuticals (Jose & Netto, 2019), cosmetic (Duprat-De-Paule et al., 2018; Patel et al., 2021) and food (Rios et al., 2014). Recently, the use of crystalline fat to produce structured oils (oleogels) has gained significant attention from academia and industry alike, due to the potential to produce solid-like materials with low amounts of saturated fat and specific macroscopic properties (Patel & Dewettinck, 2016). Furthermore, oleogels may be used as precursors for the production of oil-continuous foams (Binks & Vishal, 2021) and emulsified oil foams (Brun et al., 2015; Goibier et al., 2019) that can find application as nutrients or drug delivery vehicles, or as structuring materials for food products. In all of the above examples, the properties of the fat crystals, such as crystal size, shape and polymorphism, significantly affect the stability and functionality (*e.g.*, drug delivery, oil binding capacity, air incorporation) of the final oleogel

material (Co & Marangoni, 2012; Heymans et al., 2017). The total amount of crystals, *i.e.* the solid fat content (*SFC*%), is a general parameter strongly related to some macroscopic properties of fat-based materials, such as the melting point, hardness and texture (Himawan et al., 2006). Hence, monitoring *SFC*% during crystallization processes is important to determine when equilibrium conditions are reached, and therefore maximize the yield of crystallization in industrial contexts.

The *SFC*% is routinely measured by means of nuclear magnetic resonance (NMR) (Cerdeira et al., 2004), differential scanning calorimetry (DSC) (Foubert et al., 2008) or small-angle X-Ray scattering (SAXS) (Ladd Parada et al., 2019). These techniques, however, are all off-line, requiring the collection of a sample (not always a trivial operation, especially if the sample melting point is close to ambient temperature) and some degree of sample preparation, which can significantly affect the measurement. In the context of industrial large-scale crystallization, the issues related to off-line analysis and sampling are tackled by applying process analytical technology (PAT) tools, which enable real-time monitoring of the product properties, enhanced process understanding, and the application of the so called "Quality by Design" (QbD) strategy (Rathore et al., 2010). Common PAT tools used to monitor crystallization usually include *in situ* probes that exploit the scattering or absorption of electromagnetic radiation (visible light, ultra-violet (UV) or infra-red) by the sample to monitor phase transitions, polymorphic transformations or crystal morphology (Hansen et al., 2017; Simone et al., 2015; Simone et al., 2019). In the case of industrial lipid crystallization, online determination of the *SFC%* is highly sought, albeit presenting some challenges. Fat crystals form a viscous three-dimensional network of aggregates with a fractal pattern (Tang & Marangoni, 2008), whose quantification is non-trivial. Moreover, (partially) crystalline fat is often opaque to electromagnetic radiation, limiting the analysis to the surface of the sample. While oleogels (and hydrogels) are widely used in consumer products, at present there

63 are sparse examples of PAT tools applied to the manufacturing process of materials with similar
64 properties (Bostijn et al., 2018; Pu et al., 2015).

65 The use of low-power ultrasound for studying the crystallization of lipids has been proposed as a
66 non-invasive, non-destructive method since the 1980s (Hussin & Povey, 1984; McClements &
67 Povey, 1988; McClements & Povey, 1987). Low-power ultrasound, *i.e.,* sound waves exceeding
68 20 kHz frequency, can penetrate opaque media, without causing physical and chemical changes in
69 the sample. Moreover, it is relatively inexpensive compared to other spectroscopy techniques, and
70 it is easily adaptable to different measuring configurations (Povey, 2017). The technique involves
71 the propagation of a short (few microseconds) ultrasonic pulse from a transducer into the sample;
72 this pulse is received by either another transducer on the other side of the measuring apparatus
73 (pitch-and-catch mode) or it is reflected and received by the same emitting transducer (pulse-echo
74 mode). The velocity of sound (c_{sample}) is then calculated from the travelled path length as a function
75 of time and temperature. The acoustic attenuation (α), *i.e.,* the ratio of the amplitude of the sent
76 and received pulse, may also be calculated. As both the velocity of sound and acoustic attenuation
77 depend on the physicochemical properties of the sample, such as density and adiabatic
78 compressibility, and the presence of heterogeneities, acoustic measurements can be used to
79 monitor phase transitions such as crystallization and polymorphic transformations (Fairley &
80 McClements, 1992; Kloek et al., 2000; Miles et al., 1985). Several authors demonstrated the use
81 of custom-made acoustic cells to study fat crystallization using acoustic signals, with particular
82 emphasis on determining the *SFC*(%) (Birkhofer et al., 2008; Martini et al., 2005a, Martini et al.,
83 2005b; Singh et al., 2002, Singh et al., 2004). Nevertheless, most of the previous works on fat
84 crystallization were carried out in quiescent conditions, and/or with small sample volumes, thus

85 excluding the effect of shear and secondary nucleation on crystallization which are predominant
86 on industrial scale (Agrawal & Paterson, 2015).

87 Despite its several advantages and ease of implementation, there are only sporadic examples in the
88 literature on the use of acoustic probes as a PAT tool for studying lipid crystallization. The
89 immersion probe described in Titiz-Sargut & Ulrich (2003), which featured two 2 MHz
90 transducers in pitch-and-catch mode, was applied to the determination of the metastable zone
91 width (MSZW) of coconut oil, and validated by optical back-reflectance measurements (ORM)
92 (Chaleepa et al., 2010). The authors focused their study on the effect of different levels of shear,
93 cooling rates and the presence of additives on the MSZW; however, no quantitative information
94 on the *SFC%* of this lipid system was reported. Due to the complexity involved in the
95 crystallization of lipids, such as the occurrence of melt-mediated polymorphic transformations,
96 and the development of crystalline networks whose size range from nanometres to several
97 hundreds of microns, the determination of the SFC% directly from acoustic parameters is non-
98 trivial. Moreover, the large acoustic attenuation exhibited by crystalline fat results often in loss of
99 the acoustic signal (Rigolle et al., 2018). One of the growing trends in the use of PAT tools is the
100 implementation of machine learning (ML) algorithms to facilitate analysis of real-time data
101 provided by sensors, and to enable prediction of material properties of interest based on training
102 the algorithm with known outcomes (supervised machine learning) (Wasalathanthri et al., 2020).
103 Examples of ML applications in the context of crystallization include the automatic detection of
104 crystal aggregation from microscopic images (Ochsenbein et al., 2015), the real-time estimation
105 of the crystal size distribution of 2D needle-shaped crystals from measurements of chord length
106 and aspect ratio distributions (Szilágyi & Nagy, 2018) and the estimation of the 3D size
107 distribution of plate-like particles using projections from multiple cameras (Jaeggi et al., 2021).

The approach can be extended to the actual control of crystallization processing, for example through the use of convolutional neural network (CNN) feedback control to dissolve undesired precipitated impurities during the crystallization of active pharmaceutical ingredients (APIs) (Salami et al., 2021). Recently, ML has been applied to ultrasonic reflectance measurements to monitor the mixing process in a large-scale vessel (Bowler et al., 2020; Bowler & Watson, 2021).

In this work, a novel technique for estimating the *SFC%*, based on a custom-built acoustic probe (Morris et al., 2021) and supervised machine learning is presented. This immersion acoustic probe was used as a PAT sensor to monitor the crystallization of a cocoa butter/sunflower oil oleogel system, in a 1L scale vessel and under shear. Stirring was maintained constant throughout the whole temperature profile. Cocoa butter and sunflower oil are both ingredients widely used in food, cosmetic and pharmaceutical applications (Metilli et al., 2021). The ultrasonic data was validated with light turbidimetry, and the *SFC%* of the crystallized oleogel was measured with offline pulsed NMR (*p*NMR) at equilibrium conditions and specific temperatures. Finally, supervised machine learning was applied to develop a predictive model based on the acoustic parameters and the results of *p*NMR, enabling the calculation of *SFC%* based on the velocity of sound, sample composition and temperature.

2. Materials and Methods

2.1 Cocoa butter–based oleogels

Refined, bleached and deodorized cocoa butter (CB) and high-oleic sunflower oil (HOSO) were kindly provided by Nestlé PTC Confectionery (York, UK) and used without any further purification. CB was melted at 65 °C for one hour, and then mixed with HOSO at 9%, 11%, 13% and 15% concentration by weight. HOSO contains usually the following fatty acids (by weight):

86% oleic acid, 5% stearic acid, 3% linoleic acid, 3% palmitic acid, 1.5% behenic acid, and 0.7% arachidic acid. CB normally contains by a weight about 26% palmitic acid, 36% stearic acid, 34% oleic acid, 2.7% linoleic, and 0.9% arachidic acid.

2.2 Fat crystallization rig

The CB-HOSO mixture (900 g) was transferred to a jacketed crystallization vessel (capacity *ca.*1 L, diameter 15 cm) (Radley, UK) connected to a Huber Ministat 230 thermostat (Huber, Germany), filled with silicone oil as a heating/cooling medium. The sample was stirred continuously at 200 rpm with a DLH overhead stirrer (VELP Scientifica, Italy), equipped with an anchor-shaped mixer (8 cm diameter). A Pt-100 temperature probe (Omega Engineering, UK), placed in the vessel, was used to monitor the sample temperature during the experiment. The crystallization process was followed using a Control 4000 turbidity meter (Optek, Germany) fitted with an ASD12-N absorption probe, which measured light transmittance and absorbance. Finally, the velocity of sound and the acoustic attenuation of the crystallizing mixture were measured using a custom acoustic probe, recently described in literature (Morris et al., 2021), with some design modifications. Briefly, the probe comprised a 2.25 MHz broadband transducer coupled with a Rexolite buffer rod (Sonatest model RDT5025, Sonatest, UK), and a stainless-steel acoustic reflector plate. This probe was manufactured in an 'L' shape configuration. The probe was connected to a UT320 pulser/receiver (UTEX scientific instruments inc., Canada) and a HDO3034 digital oscilloscope (Teledyne LeCroy, USA). A schematic of the equipment is shown in Figure 1.

The thermal profile of the experiment was set to the following: Equilibration of the fat blend mixture at 45 °C for 10 minutes, cooling to 0 °C at a nominal rate of –0.5 °C/min and holding at

0°C for 3 hours. The sample was then heated back to 45 °C at 1 °C/min. The process temperature and the acoustic waveforms were collected using an in-house script developed with MATLAB2021a (MathWorks, USA). Measurements were collected every 10 seconds. Each experiment was repeated three times.

2.3 Determination of the acoustic parameters

2.3.1 Velocity of Sound

Figure contains a diagram describing the design of the acoustic probe, and an example of waveform acquired from the oscilloscope with MATLAB.

The ultrasonic pulse generated from the transducer travels through the buffer rod, and it is partially reflected at the buffer rod/sample interface, due to the acoustic impedance mismatch (*i.e.*, the difference in the product of density and velocity of sound of the two materials). The pulse is then received back by the transducer after a time Δt_1, shown in Figure as the blue trace. Part of the initial pulse, however, is transmitted through the sample, and it is reflected by the stainless-steel reflector to the transducer after a time Δt_2 (Figure , red trace). In order to calculate the velocity of sound in the sample, the time of flight in the sample is required. To calculate it, the initial value of Δt_1 and Δt_2 were first determined with MATLAB from the original waveform, using the leading-edge method (*i.e.*, detecting the arrival time of the pulse envelope when it crosses a set voltage threshold). Afterwards, the shifts of the pulses' position ($\Delta\Delta t_1$ and $\Delta\Delta t_2$) during the experiment were calculated with the cross-correlation function (*xcorr*) implemented in MATLAB. This function provides an estimate of the correlation between each analysed waveform and a reference waveform, returning the intensity of the correlation value as a function of time units. The position of the maximum peak of this calculated vector corresponds to the time delay between two pulses. This method proved to be more robust in the analysis of the set of waveforms compared to applying

the leading-edge technique on all collected waveforms. This is because the pulse envelop was subject to distortion due to frequency dependent signal attenuation through the experiment. The variation in the sample time of flight ($\Delta\Delta t_3$) was then calculated with Equation 1:

$$\Delta\Delta t_3 = \Delta\Delta t_2 - \Delta\Delta t_1 \quad \text{(Eq. 1)}$$

In order to obtain an accurate value of the velocity of sound, however, it was necessary to determine the path length dependence on the temperature with a calibration experiment. The velocity of sound in distilled water (c_{water}) with respect to temperature (T) may be calculated using a fifth-order polynomial, as first described by Chávez et al. (1985) (Equation 2):

$$c_{water} = 3.16 \cdot 10^{-9}T^5 - 1.48 \cdot 10^{-6}T^4 + 3.35 \cdot 10^{-4}T^3 - 5.81 \cdot 10^{-2}T^2 + 5.04 \cdot T + 1.40 \cdot 10^3 \quad \text{(Eq. 2)}$$

The shift in the time of flight in distilled water ($\Delta\Delta t_{3,\text{water}}$) was then measured between 50 °C and 5°C, using a –0.01 °C/min cooling rate to allow the probe to reach thermal equilibrium with the surrounding medium. The corresponding experimental path length ($L_{\text{calibrated}}$) was calculated with Equation 3

$$L_{calibrated} = \Delta\Delta t_{3,water} \times c_{water} \quad \text{(Eq. 3)}$$

The dependence of the path length on the temperature was then obtained by fitting a fifth-order polynomial to $L_{\text{calibrated}}$ against the temperature (Figure).

The coefficients estimated for the path length calculation were then used to accurately calculate the velocity of sound during the crystallization experiments with Equation 4

$$c_{sample} = \frac{L_{calibrated}}{\Delta\Delta t_3} \quad \text{(Eq. 4)}$$

2.3.2 Acoustic Attenuation

The acoustic attenuation quantifies the acoustic power absorbed and scattered by the sample, and is affected by several factors, including the onset of phase transitions and scattering phenomena

generated by the presence of dispersed objects in the sample (McClements & Povey, 1992). In this work, the acoustic attenuation was used to detect the onset of crystal growth and dissolution during the crystallization experiments. The acoustic attenuation was calculated according to Equation 5

$$\alpha = -20 \log \frac{A}{A_0} \quad \text{(Eq. 5)}$$

where A and A_0 are the peak-to-peak amplitudes of the sample signal during the experiment, and at the start of the experiment, respectively.

2.3.3 Solid Fat Content

The solid fat content (*SFC*%), defined as the mass fraction of solid to liquid material in a fat blend, was calculated by applying a prediction model, developed with the Regression Learner App in MATLAB2021a, (MathWorks, USA). Regression Learner is a supervised machine-learning utility, where a regression algorithm is applied to an observation matrix and compared with a response matrix. The observation matrix comprised the temperature (T), velocity of sound in the sample (c_{sample}) and the amount of added cocoa butter (CB%) for each crystallization experiment; the response matrix contained the *SFC*% values, measured with pNMR, between 5 and 45 °C for the respective samples. The velocity of sound and temperature of pure sunflower oil were also added to the observation matrix, with a corresponding solid fat content of 0%. The sunflower oil data was included in the model to provide information on the behaviour of a sample without any crystallizing material in the explored experimental conditions. Three models available in the Regression Learner App were tested for training of the dataset, and their predictive ability were compared: “Linear”, “Fine Tree” and “Gaussian Process Regression–Rational Quadratic”. The Linear model uses a linear regression to fit the data from the observation matrix. The “Fine Tree” model, instead, is a type of nonlinear model based on regression trees, which applies a recursive

partition of the observation matrix to improve the prediction of the response value. Lastly, the Gaussian Process Regression model, which is also nonlinear, works by predicting the probability distribution of responses for each parameter in the observation matrix. Model cross-validation was performed using the in-built function in the Regression Learner App (5-fold validation setting). Briefly, the software divides the dataset into a number of sub-sets of the same size, trains the predictive model on all sub-sets except one, which is used as test data. This process is repeated until all sub-sets have been used as test data once (Bosnić & Kononenko, 2009). The accuracy of all iterations is calculated as R^2, RMSE and other statistical parameters. In the discussion, the Root Mean Square Error values (RMSE) were compared to select the most accurate predictive model.

In addition to the predictive model, an equation that estimates the equilibrium *SFC*% as function of the temperature and the concentration of CB in sunflower oil was determined using the *Curve Fitting Tool* in MATLAB2021a. A custom equation based on literature was used to fit the experimental data using the *NonlinearLeastSquares* method; R^2, RMSE and 95% confidence intervals for each estimated parameters were also calculated.

2.4 Pulsed Nuclear Magnetic Resonance (pNMR)

The solid fat content (*SFC*%) of the CB-HOSO mixtures was determined with *p*NMR using a Bruker Minispec NMR (Bruker, Switzerland). The samples were collected at the end of the crystallization experiment, transferred to a 10 mm inner diameter NMR tube and stored in a fridge at 4 °C. The *SFC*% was measured between 5 and 45 °C, in steps of 5 °C. During the experiment, the NMR tube was left to equilibrate for 90 minutes for each temperature step. The measurements were carried out in triplicates. The resulting *SFC(%)* vs. temperature data was fitted using a Gompertz-type model (Farmani, 2015) to obtain the *SFC(%)* as a function of the temperature and CB%.

3. Results and Discussion

3.1 Fat crystallization monitored by PAT tools

The crystallization of one 9% CB w/w in HOSO sample, monitored with turbidity and the acoustic probe, is shown in Figure 4.

While some variability among the three experiments conducted for each CB concentration was observed, (particularly in the crystallization temperature and the absolute values of acoustic attenuation) the trends observed for all CB/HOSO samples were similar. In particular, for the experiment shown in Figure 4a, four regions could be identified. Between 0 and 115 minutes (region I of Figure 4a) the temperature of the sample followed the cooling profile, from 45 °C to 5°C, accompanied by an increase in the velocity of sound, from 1390 to 1510 m/s, due to the negative velocity coefficient with respect to temperature (McClements & Povey, 1992). After 115 minutes, when the sample temperature reached 5 °C, the onset of nucleation was detected by a sharp decrease in the light transmittance, due to the sample becoming turbid (region II). Simultaneously, the light absorbance increased, exhibiting two distinct steps: a first, modest increase occurring between 115 and 129 minutes, and a larger increase after 129 minutes. Interestingly, the acoustic attenuation and the velocity of sound were responsive to the second step only, with a delay in detecting the onset of crystallization of *ca.* 14 minutes. This behaviour was consistently observed across all CB % w/w concentrations (Figure S1 of Supporting Information), and reported also in previous works (Martini et al., 2005b; Singh et al., 2002). The sheared crystallization of CB/HOSO mixtures was thoroughly investigated in a recent publication, reporting that cocoa butter crystallized as spherical aggregates of crystalline nanoplatelet (CNPs) in the β(V) form (Metilli et al., 2021) (Figure 5). Additional characterization is provided in the Supporting Information (Figure S2).

It is hypothesized, however, that CB first nucleated as a metastable polymorph (α or β') and then transformed into the β(V) structure during the experiments. It might be that the change in compressibility and/or density associated to the formation of a liquid crystal structure – most likely the α polymorph – were too small to be detected by the acoustic probe used in this work (Ladd Parada et al., 2019). On the other hand, the nucleation and the growth of the β (V) crystals and the consequent development of the fat crystal network were clearly detected in both the velocity of sound and acoustic attenuation (at 129 minutes). As the velocity of sound depends strongly on the temperature, the first derivative with respect to temperature was calculated to better discriminate the effect of crystal nucleation on this acoustic parameter (Figure 4b). Before the appearance of fat crystals, when the change in the velocity of sound was only dependent on the temperature, the calculated first derivative was zero; whereas, upon growth of the CB crystal network, the value of this parameter changed significantly. Variations in the first derivative occurred at the same time with the increase of the acoustic attenuation, which was caused by (a) scattering by fat crystals and (b) additional attenuation mechanisms associated with the space filling interconnected fat crystals, which also affected the overall compressibility of the system through the appearance of an additional 'frame modulus' (Povey, 2017). Finally, fat crystal nucleation might release a high amount of latent heat of solidification. In the case of the experiment of Figure 4a, such exothermic process increased the process temperature from 3.2 °C to 5.65 °C (130-137 minutes). While this temperature perturbation did not affect the signal from the turbidity probe or the acoustic attenuation, it did affect the velocity of sound, which is strongly dependent on the sample temperature.

After nucleation of the β(V) polymorph, the crystallization process of Figure 4a proceeded until 275 minutes (region III), when the sample temperature reached *ca.* 1.5 °C, which corresponded to

285 the thermal equilibrium of the whole setup. In this time the acoustic attenuation kept increasing,
286 following a similar trend to the light absorbance. The velocity of sound also increased, but mostly
287 due to the change in temperature. Nevertheless, it is worth noticing in Figure 4b that the appearance
288 of fat crystals determined an increase in the noise of the first derivative of the velocity of sound,
289 albeit its mean value was still around zero.
290 After reaching equilibrium at around 275 minutes, the sample was heated back to 45 °C (region
291 IV). A focus on this region of the experiment is displayed in Figure 4c. In the heating step between
292 1.5 °C to 15 °C (from 280 minutes to 315 minutes), a decrease in the velocity of sound linearly
293 proportional to the decrease in temperature was observed. At the same time, a moderate decrease
294 in the acoustic attenuation happened, potentially linked to a decrease in the *SFC%* of the
295 crystallized sample.
296 Further increase in the sample temperature (from 315 to 330 minutes, 15 °C to 25 °C) resulted in
297 the complete melting of the fat crystalline network, which was evident in the sharp increase in
298 light transmittance and in the decrease in light absorbance, as well as acoustic attenuation. It is
299 worth noticing that both techniques detected full dissolution at the same time, around 327 minutes.
300 The velocity of sound presented a steeper decline in correspondence to the full melting; this was
301 clearly observable in the calculated first derivative.
302 Upon complete remelting of the sample (330 minutes – 350 minutes) all parameters returned to
303 their values prior to crystallization.
304 This set of experiments showed that the tested acoustic probe could be used to monitor
305 crystallization processes, although it seemed less sensitive than light turbidimetry to the detection
306 of early nucleated crystals, perhaps due to their liquid crystalline nature.

307 Experiments carried out with a higher weight % of CB showed similar trends for the acoustic and
308 light signals. The velocity of sound of the crystallized oleogels at different % w/w of added CB,
309 between 5 and 35°C, is shown in Figure 6.
310 In agreement with previous literature (McClements & Povey, 1992), the velocity of sound of the
311 crystallized oleogels increased, for the same range of temperatures, with increasing CB % w/w
312 (approximately by 10 m/s every 2 % of CB). From Figure 6 it can be noted that, between 20 and
313 25°C, the velocity of sound of all samples decreased steeply, due to the oleogels melting. It can be
314 appreciated that such decrease occurred at lower temperatures for lower CB concentrations, in
315 accordance with the lower melting point of the oleogels. Once liquid, the oleogels then displayed
316 the same velocity of sound of the sunflower oil.
317 The acoustic attenuation measured at equilibrium also increased with the amount of CB contained
318 in the oleogel, as shown in **Table 1**. In fact, higher concentrations of crystalline solids scattered
319 more sound and attenuated it. The relatively large standard deviation of the acoustic attenuation
320 for the 9% CB w/w sample, and its non-linear increase with higher concentrations of CB w/w,
321 however, prompts further work to establish a more robust relationship with the amount of solid fat
322 in the sample. In fact, the relationship between acoustic attenuation, SFC(%) and the crystal size
323 and shape is challenging to elucidate (Martini et al., 2005a).
324 The solid fat content (*SFC%*) of the CB/HOSO samples as a function of temperature was measured
325 with *p*NMR at the end of the crystallization step (Figure 7). Samples were collected directly from
326 the vessel to ensure direct comparison with the performed experiments.
327 By inspecting the *SFC*% values at 5 °C, it can be noted that all samples displayed a lower *SFC*%
328 compared to the total amount of added cocoa butter. This is because the main triacylglycerides
329 species that are solid at ambient temperature, 1,3-dipalmitoyl-2-oleoyl-glycerol (POP), 1,3-

distearoyl-2-oleoyl-glycerol (SOS) and 1-palmitoyl-2-oleoyl-3-stearoyl-glycerol (POS), constitute about 80% w/w of cocoa butter, while the remaining 20% comprises mono- and di-glycerides, phospholipids, sterols and free fatty acids that are liquid at ambient conditions (Dimick, 1991). It is worth noticing that the *p*NMR measurements present an average standard deviation of 0.101%, which is a more than acceptable value for industrial applications (particularly the confectionary sector).

The *SFC(%)* values at equilibrium were fitted using a Gompertz-type model, similar to the one described in Farmani (2015) (Equation 6):

$$SFC(\%)(T, CB) = (b_0 + b_1 CB)e^{-e^{\frac{-\left(T-(b_{01}+(b_{11}CB))\right)}{c}}} \quad \text{(Eq. 6)}$$

where T is the sample temperature in °C, CB is the concentration (w/w) of added cocoa butter, and b_0 = 1.24, b_1 = 73, b_{01} = 13.48, b_{11} = 38.5 and c = -4.66 are the coefficient determined via interpolation in MATLAB. The R^2 of the fitting was equal to 0.9965 with a $RMSE$ of 0.2324% (95% confidence intervals for each parameter are shown in supporting information Table S1), which is still acceptable for industrial purposes.

This fit enabled calculation of the equilibrium *SFC(%)* as a function of temperature and CB concentration, which can be used in combination with the predictive models determined in the next section for oleogels with composition ranging from 9 to 15% of CB.

3.2 Solid fat content predicted by Regression Learner model

The measured *SFC(%)* with *p*NMR, and the predicted *SFC(%)* obtained with the Regression Learner models is displayed in Figure 8.

It can be noticed how the Linear model showed inaccuracies both when the sample was in the melted state (high temperatures), as well as in its crystallized phase, at all concentrations. This

could be ascribed to the non-linear dependence of the *SFC(%)* with respect to temperature, as already highlighted in Figure 7. When considering the Fine Tree model, the accuracy generally improved, however still displaying some errors in predicting the *SFC(%)* of the oleogels, in particular between 15 and 25 °C. Finally, the GPR model showed the best predictive accuracy, for all samples and temperatures, with an RMSE value almost one order of magnitude lower compared to the other two models. Such improvement could stem from the similarity between the Gompertz-type *SFC(%)* dependence with temperature (Equation 6) and the gaussian-type distribution function (also exponential). Therefore, the GPR model was selected to predict the SFC% evolution during fat crystallization, as shown in Figure .

The increase in the predicted value of the *SFC%* in the oleogel matched the increase in the acoustic attenuation at 130 minutes, reaching 5% over few minutes and then levelling to a value of about 7.6%, very close to the equilibrium *SFC%* at such temperature (as shown in Figure 7). During the heating phase, the *SFC*% started decreasing, falling sharply to 0% when the temperature was raised above 20 °C and remaining constant thereafter, until the end of the experiment. Therefore, in contrast with previous research, the approach presented in this work only requires measuring velocity of sound, the temperature, and the *SFC(%)* measured with *p*NMR on samples on the concentration of interest. The *SFC(%)* is then rapidly and accurately predicted from the ultrasonic probe data under realistic operating conditions (*i.e.*, under shear and with large sample volumes).

The predicted *SFC*% for the samples at different CB % was plotted as a function of temperature in Figure .

By inspecting the cooling profile, it can be noted that crystal growth, signalled by the increase in *SFC*%, occurred at higher crystallization temperatures for oleogels containing higher % of CB, as also reported previously in Metilli et al. (2021) for this type of system. Whereas, by inspecting the

heating profile, the *SFC*% decreased with the temperature with the same trend observed with *p*NMR. The estimated values of *SFC%* at 5 °C during heating were 7.3, 8.7, 10.2 and 11.7% for the 9, 11, 13 and 15% CB samples, respectively. These values are very close to the equilibrium SFC% measured with *p*NMR at the same temperature (7.6, 8.5, 10.3 and 11.7%) indicating the reliability of the predictive model built. Furthermore, both *p*NMR and acoustic spectroscopy showed agreement that at 25 °C all samples returned to the full liquid state.

This work presents a prototype of an acoustic in situ probe, coupled with a reliable machine learning-based predictive model, for online monitoring of oleogels crystallization. The probe could provide useful quantitative information on the evolution of crystallization processes in an industrial setting with minimal investment cost and calibration experiments. Furthermore, due to the versatility of acoustic probes, the design of the hardware could be optimized in order to allow effective measurements even in different fluid-dynamic environment (e.g., different crystallizers designs, commercial tempering equipment).

4. Conclusions

In this work, the crystallization of cocoa butter–based oleogels was characterized qualitatively and qualitatively using a custom-built immersion probe based on pulsed acoustic spectroscopy. The *SFC%* of the oleogel during crystallization was estimated through a predictive model developed with supervised machine learning. Such method uses the acoustic parameters (*i.e.*, velocity of sound) collected from the immersion probe, the sample temperature and composition, and the *SFC%* measured with *p*NMR. The predicted *SFC%* and its evolution during the shear crystallization of the CB/HOSO mixtures was in agreement with the nucleation and development of crystalline fat, as corroborated by light turbidimetry and acoustic attenuation. A comparison

between several predictive models showed that Gaussian Process Regression model was the most accurate in describing the *SFC%* both prior and during crystallization. The *SFC%* value increased steeply during crystal growth, with a final value close to 80% by weight of the added cocoa butter in the mixture, with a similar trend to the acoustic attenuation. The SFC% then returned to 0% close to the melting point of the oleogel, in agreement with the melting profile measured with *p*NMR. Moreover, this work highlighted that turbidimetry was more sensitive in detecting the nucleation of lipid crystals, whereas the acoustic probe was more responsive to the crystal growth process. This difference could be ascribed to the liquid-crystalline nature of the metastable lipid polymorph that developed during nucleation, for which the change in density and compressibility may be too small to be measured by the current acoustic probe. Using a different frequency transducer might increase the sensitivity of the ultrasonic probe to crystal nucleation; however, this might result in excessive signal attenuation at equilibrium conditions, at which the *SFC*% needs to be calculated. In summary, the results presented in this work demonstrate the feasibility of implementing acoustic probes as PAT tools, in combination with supervised machine learning, to improve the oleogel crystallization yield through the timely and accurate monitoring of the *SFC%.*

ASSOCIATED CONTENT

Supporting Information.

PAT tools plot of 9, 11, 13 and 15% w/w CB in HOSO samples focused on nucleation of CB crystals (Figure S1). SAXS and WAXS patterns, DSC and CryoSEM images of a 15% w/w CB in HOSO oleogel sample (Figure S2).

AUTHOR INFORMATION

Corresponding Author

Prof. Elena Simone

Elena.simone@polito.it

Author Contributions

The manuscript was written through contributions of all authors. All authors have given approval to the final version of the manuscript.

Funding Sources

Centre for Doctoral Training in Soft Matter and Functional Interfaces (Grant ref. no. EP/L015536/1).

Royal Society (Grant ref. no. INF\R2\192018).

Royal Academy of Engineering (Grant ref. no. IF/192031).

ACKNOWLEDGMENTS

The authors would like to acknowledge the Engineering and Physical Sciences Research Council funded Centre for Doctoral Training in Soft Matter and Functional Interfaces, grant ref. no. EP/L015536/1 as well as Nestlé PTC Confectionery (York, UK) for the pulsed NMR analysis, and the financial and writing support. E.S. also acknowledges Royal Society (Grant ref. no.

INF\R2\192018) and Royal Academy of Engineering (Grant ref. no. IF/192031) for additional funding.

ABBREVIATIONS

CB cocoa butter, GPR gaussian process regression, HOSO high oleic sunflower oil, ML machine learning, SFC solid fat content, PAT process analytical technologies, *p*NMR pulsed nuclear magnetic resonance.

REFERENCES

Agrawal, S. G., & Paterson, A. H. J. (2015). Secondary Nucleation: Mechanisms and Models. *Chemical Engineering Communications*, *202*(5), 698–706. https://doi.org/10.1080/00986445.2014.969369

Rigolle, A., Van Den Abeele, K. and Foubert, I. (2018). Conventional and New Techniques to Monitor Lipid Crystallization. In Crystallization of Lipids, K. Sato (Ed.). https://doi.org/10.1002/9781118593882.ch17

Binks, B. P., & Vishal, B. (2021). Particle-stabilized oil foams. *Advances in Colloid and Interface Science*, *291*, 102404. https://doi.org/10.1016/j.cis.2021.102404

Birkhofer, B. H., Jeelani, S. A. K., Windhab, E. J., Ouriev, B., Lisner, K.-J., Braun, P., & Zeng, Y. (2008). Monitoring of fat crystallization process using UVP–PD technique. *Flow Measurement and Instrumentation*, *19*(3–4), 163–169. https://doi.org/10.1016/j.flowmeasinst.2007.08.008

Bosnić, Z., & Kononenko, I. (2009). An overview of advances in reliability estimation of individual predictions in machine learning. *Intelligent Data Analysis*, *13*(2), 385–401.

https://doi.org/10.3233/IDA-2009-0371

Bostijn, N., Hellings, M., Van Der Veen, M., Vervaet, C., & De Beer, T. (2018). In-line UV spectroscopy for the quantification of low-dose active ingredients during the manufacturing of pharmaceutical semi-solid and liquid formulations. *Analytica Chimica Acta*, *1013*, 54–62. https://doi.org/10.1016/j.aca.2018.02.007

Bowler, A. L., Bakalis, S., & Watson, N. J. (2020). Monitoring Mixing Processes Using Ultrasonic Sensors and Machine Learning. *Sensors*, *20*(7), 1813. https://doi.org/10.3390/s20071813

Bowler, A. L., & Watson, N. J. (2021). Transfer learning for process monitoring using reflection-mode ultrasonic sensing. *Ultrasonics*, *115*(May), 106468. https://doi.org/10.1016/j.ultras.2021.106468

Brun, M., Delample, M., Harte, E., Lecomte, S., & Leal-Calderon, F. (2015). Stabilization of air bubbles in oil by surfactant crystals: A route to produce air-in-oil foams and air-in-oil-in-water emulsions. *Food Research International*, *67*, 366–375. https://doi.org/10.1016/j.foodres.2014.11.044

Cerdeira, M., Candal, R.J., Herrera, M. L. (2004). Analytical Techniques for Nucleation Studies in Lipids : Advantages and Disadvantages. *Journal of Food Science*, *69*(9), R185–R191.

Chaleepa, K., Szepes, A., & Ulrich, J. (2010). Metastable zone determination of lipid systems: Ultrasound velocity versus optical back-reflectance measurements. *European Journal of Lipid Science and Technology*, *112*(5), 565–573. https://doi.org/10.1002/ejlt.200900225

Chávez, M., Sosa, V., & Tsumura, R. (1985). Speed of sound in saturated pure water. *Journal of the Acoustical Society of America*, *77*(2), 420–423. https://doi.org/10.1121/1.391861

Co, E. D., & Marangoni, A. G. (2012). Organogels: An alternative edible oil-structuring method. *JAOCS, Journal of the American Oil Chemists' Society*, *89*(5), 749–780. https://doi.org/10.1007/s11746-012-2049-3

Dimick, P. S. (1991). Principles of cocoa butter crystallization. *Manufacturing Confectioner*, *71*(5), 115–125.

Duprat-De-Paule, S., Guilbot, J., Roso, A., Cambos, S., & Pierre, A. (2018). Augmented bio-based lipids for cosmetics. *OCL - Oilseeds and Fats, Crops and Lipids*, *25*(5). https://doi.org/10.1051/ocl/2018036

Fairley, P., & McClements, D. J. (1992). Frequency scanning ultrasonic pulse echo reflectometer. *Ultrasonics*, *30*(6), 403–405.

Farmani, J. (2015). Modeling of solid fat content of chemically interesterified fully hydrogenated soybean oil and canola oil blends as a function of temperature and saturated fatty acids. *Journal of Food Measurement and Characterization*, *9*(3), 281–289. https://doi.org/10.1007/s11694-015-9233-8

Fernández-Moya, V., Martínez-Force, E., & Garcés, R. (2000). Identification of triacylglycerol species from high-saturated sunflower (Helianthus annuus) mutants. *Journal of Agricultural and Food Chemistry*, *48*(3), 764–769. https://doi.org/10.1021/jf9903861

Foubert, I., Fredrick, E., Vereecken, J., Sichien, M., & Dewettinck, K. (2008). Stop-and-return DSC method to study fat crystallization. *Thermochimica Acta*, *471*(1–2), 7–13. https://doi.org/10.1016/j.tca.2008.02.005

Goibier, L., Pillement, C., Monteil, J., Faure, C., & Leal-Calderon, F. (2019). Emulsification of

non-aqueous foams stabilized by fat crystals: Towards novel air-in-oil-in-water food colloids. *Food Chemistry*, *293*, 49–56. https://doi.org/10.1016/j.foodchem.2019.04.080

Hansen, T. B., Simone, E., Nagy, Z., & Qu, H. (2017). Process Analytical Tools to Control Polymorphism and Particle Size in Batch Crystallization Processes. *Organic Process Research and Development*, *21*(6), 855–865. https://doi.org/10.1021/acs.oprd.7b00087

Heymans, R., Tavernier, I., Dewettinck, K., & Van der Meeren, P. (2017). Crystal stabilization of edible oil foams. *Trends in Food Science and Technology*, *69*, 13–24. https://doi.org/10.1016/j.tifs.2017.08.015

Himawan, C., Starov, V. M., & Stapley, A. G. F. (2006). Thermodynamic and kinetic aspects of fat crystallization. *Advances in Colloid and Interface Science*, *122*, 3–33. https://doi.org/10.1016/j.cis.2006.06.016

Hussin, A. B. B. H., & Povey, M. J. W. (1984). A study of dilatation and acoustic propagation in solidifying fats and oils: II. Experimental. *Journal of the American Oil Chemists' Society*, *61*(3), 560–564. https://doi.org/10.1007/BF02677032

Jaeggi, A., Rajagopalan, A. K., Morari, M., & Mazzotti, M. (2021). Characterizing Ensembles of Platelike Particles via Machine Learning. *Industrial & Engineering Chemistry Research*, *60*(1), 473–483. https://doi.org/10.1021/acs.iecr.0c04662

Jose, J., & Netto, G. (2019). Role of solid lipid nanoparticles as photoprotective agents in cosmetics. *Journal of Cosmetic Dermatology*, *18*(1), 315–321. https://doi.org/10.1111/jocd.12504

Kloek, W., Walstra, P., & Van Vliet, T. (2000). Nucleation kinetics of emulsified triglyceride

mixtures. *JAOCS, Journal of the American Oil Chemists' Society*, *77*(6), 643–652. https://doi.org/10.1007/s11746-000-0104-7

Ladd Parada, M., Povey, M. J., Vieira, J., Rappolt, M., & Ries, M. E. (2019). Early stages of fat crystallisation evaluated by low-field NMR and small-angle X-ray scattering. *Magnetic Resonance in Chemistry*, *57*(9), 686–694. https://doi.org/10.1002/mrc.4860

Lipp, M., Simoneau, C., Ulberth, F., Anklam, E., Crews, C., Brereton, P., … Wiedmaier, C. (2001). Composition of genuine cocoa butter and cocoa butter equivalents. *Journal of Food Composition and Analysis*, *14*(4), 399–408. https://doi.org/10.1006/jfca.2000.0984

Martini, S., Bertoli, C., Herrera, M. L., Neeson, I., & Marangoni, A. (2005a). Attenuation of ultrasonic waves: Influence of microstructure and solid fat content. *JAOCS, Journal of the American Oil Chemists' Society*, *82*(5), 319–328. https://doi.org/10.1007/s11746-005-1073-6

Martini, S., Bertoli, C., Herrera, M. L., Neeson, I., & Marangoni, A. (2005b). In situ monitoring of solid fat content by means of pulsed nuclear magnetic resonance spectrometry and ultrasonics. *JAOCS, Journal of the American Oil Chemists' Society*, *82*(5), 305–312. https://doi.org/10.1007/s11746-005-1071-8

McClements, D. J. J., & Povey, M. J. W. (1988). Ultrasonic velocity measurements in some liquid triglycerides and vegetable oils. *Journal of the American Oil Chemists' Society*, *65*(11), 1787–1790. https://doi.org/10.1007/BF02542383

McClements, D. J., & Povey, M. J. W. (1992). Ultrasonic analysis of edible fats and oils. *Ultrasonics*, *30*(6), 383–388. https://doi.org/10.1016/0041-624X(92)90094-3

McCLEMENTS, D. J., & POVEY, M. J. W. (1987). Solid fat content determination using ultrasonic velocity measurements. *International Journal of Food Science & Technology*, *22*(5), 491–499. https://doi.org/10.1111/j.1365-2621.1987.tb00514.x

Metilli, L., Lazidis, A., Francis, M., Marty-Terrade, S., Ray, J., & Simone, E. (2021). The Effect of Crystallization Conditions on the Structural Properties of Oleofoams Made of Cocoa Butter Crystals and High Oleic Sunflower Oil. *Crystal Growth & Design*, *21*(3), 1562–1575. https://doi.org/10.1021/acs.cgd.0c01361

Miles, C. A., Fursey, G. A. J., & Jones, R. C. D. (1985). Ultrasonic estimation of solid/liquid ratios in fats, oils and adipose tissue. *Journal of the Science of Food and Agriculture*, *36*(3), 215–228. https://doi.org/10.1002/jsfa.2740360312

Morris, L., Simone, E., Glover, Z. J., Powell, H., Marty-Terrade, S., Francis, M., & Povey, M. J. (2021). Dynamic monitoring of glycine crystallisation with low power ultrasound reflection spectroscopy. *Chemical Engineering Research and Design*, *170*, 213–223. https://doi.org/10.1016/j.cherd.2021.04.003

Ochsenbein, D. R., Vetter, T., Schorsch, S., Morari, M., & Mazzotti, M. (2015). Agglomeration of needle-like crystals in suspension: I. Measurements. *Crystal Growth and Design*, *15*(4), 1923–1933. https://doi.org/10.1021/acs.cgd.5b00094

Patel, A. R., & Dewettinck, K. (2016). Edible oil structuring: An overview and recent updates. *Food and Function*, *7*(1), 20–29. https://doi.org/10.1039/c5fo01006c

Patel, D., Patel, B., & Thakkar, H. (2021). Lipid Based Nanocarriers: Promising Drug Delivery System for Topical Application. *European Journal of Lipid Science and Technology*, *123*(5),

1–12. https://doi.org/10.1002/ejlt.202000264

Povey, M. J. W. (2017). Applications of ultrasonics in food science - novel control of fat crystallization and structuring. *Current Opinion in Colloid and Interface Science*, *28*, 1–6. https://doi.org/10.1016/j.cocis.2016.12.001

Pu, Y., Chaudhry, S., Parikh, M., & Berry, J. (2015). Drug Development and Industrial Pharmacy Application of in-line viscometer for in-process monitoring of microcrystalline cellulose-carboxymethylcellulose hydrogel formation during batch manufacturing Application of in-line viscometer for in-process monitoring of microcrystalline cellulose-carboxymethylcellulose hydrogel formation during batch manufacturing. *Drug Dev Ind Pharm*, *41*(1), 28–34. https://doi.org/10.3109/03639045.2013.845837

Rathore, A. S., Bhambure, R., & Ghare, V. (2010). Process analytical technology (PAT) for biopharmaceutical products. *Analytical and Bioanalytical Chemistry*, *398*(1), 137–154. https://doi.org/10.1007/s00216-010-3781-x

Rios, R. V., Pessanha, M. D. F., Almeida, P. F. de, Viana, C. L., & Lannes, S. C. da S. (2014). Application of fats in some food products. *Food Science and Technology (Campinas)*, *34*(1), 3–15. https://doi.org/10.1590/s0101-20612014000100001

Salami, H., McDonald, M. A., Bommarius, A. S., Rousseau, R. W., & Grover, M. A. (2021). In Situ Imaging Combined with Deep Learning for Crystallization Process Monitoring: Application to Cephalexin Production. *Organic Process Research and Development*, *25*(7), 1670–1679. https://doi.org/10.1021/acs.oprd.1c00136

Simone, E., Saleemi, A. N., & Nagy, Z. K. (2015). In situ monitoring of polymorphic

transformations using a composite sensor array of Raman, NIR, and ATR-UV/vis spectroscopy, FBRM, and PVM for an intelligent decision support system. *Organic Process Research and Development*, *19*(1), 167–177. https://doi.org/10.1021/op5000122

Simone, Elena, Tyler, A. I. I., Kuah, D., Bao, X., Ries, M. E., & Baker, D. (2019). Optimal Design of Crystallization Processes for the Recovery of a Slow-Nucleating Sugar with a Complex Chemical Equilibrium in Aqueous Solution: The Case of Lactose. *Organic Process Research & Development*, *23*(2), 220–233. https://doi.org/10.1021/acs.oprd.8b00323

Singh, A. P., McClements, D. J., & Marangoni, A. G. (2002). Comparison of ultrasonic and pulsed NMR techniques for determination of solid fat content. *JAOCS, Journal of the American Oil Chemists' Society*, *79*(5), 431–437. https://doi.org/10.1007/s11746-002-0501-y

Singh, A. P., McClements, D. J., & Marangoni, A. G. (2004). Solid fat content determination by ultrasonic velocimetry. *Food Research International*, *37*(6), 545–555. https://doi.org/10.1016/j.foodres.2003.12.010

Szilágyi, B., & Nagy, Z. K. (2018). Aspect Ratio Distribution and Chord Length Distribution Driven Modeling of Crystallization of Two-Dimensional Crystals for Real-Time Model-Based Applications. *Crystal Growth & Design*, *18*(9), 5311–5321. https://doi.org/10.1021/acs.cgd.8b00758

Tang, D., & Marangoni, A. G. (2008). Fractal dimensions of simulated and real fat crystal networks in 3D space. *JAOCS, Journal of the American Oil Chemists' Society*, *85*(6), 495–499. https://doi.org/10.1007/s11746-008-1237-7

Titiz-Sargut, S., & Ulrich, J. (2003). Application of a protected ultrasound sensor for the

608 determination of the width of the metastable zone. *Chemical Engineering and Processing:*
609 *Process Intensification*, *42*(11), 841–846. https://doi.org/10.1016/S0255-2701(02)00215-5

610 Wasalathanthri, D. P., Rehmann, M. S., Song, Y., Gu, Y., Mi, L., Shao, C., … Li, Z. J. (2020).
611 Technology outlook for real-time quality attribute and process parameter monitoring in
612 biopharmaceutical development—A review. *Biotechnology and Bioengineering*, *117*(10),
613 3182–3198. https://doi.org/10.1002/bit.27461

614

615

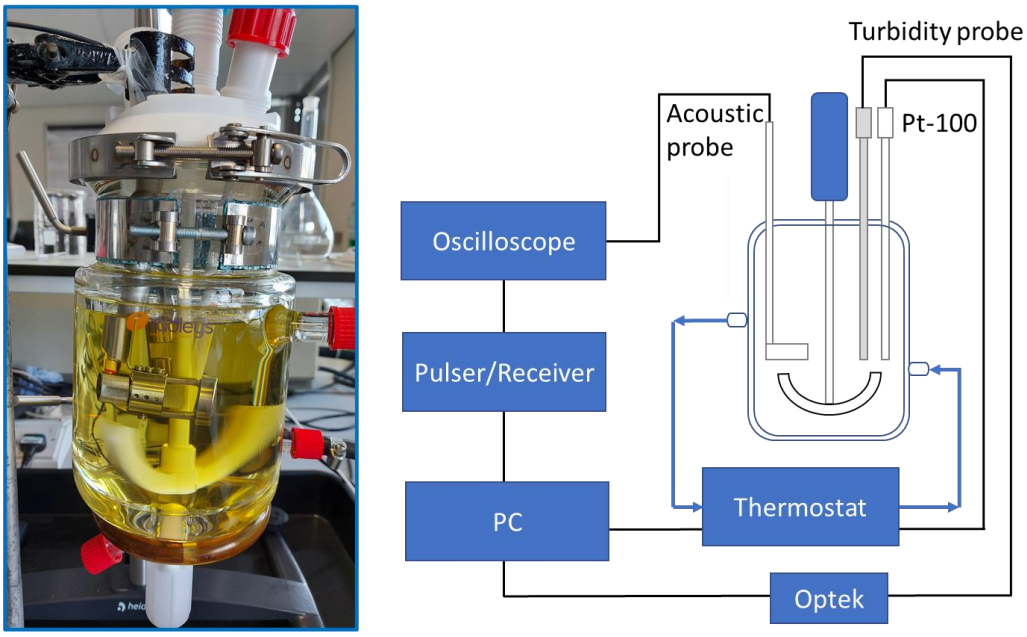

616

617 Figure 1. Crystallization vessel fitted with a Pt-100 thermocouple, the turbidity probe and the
618 custom ultrasound probe (left), schematic depiction of the rig used in this paper (right).

619

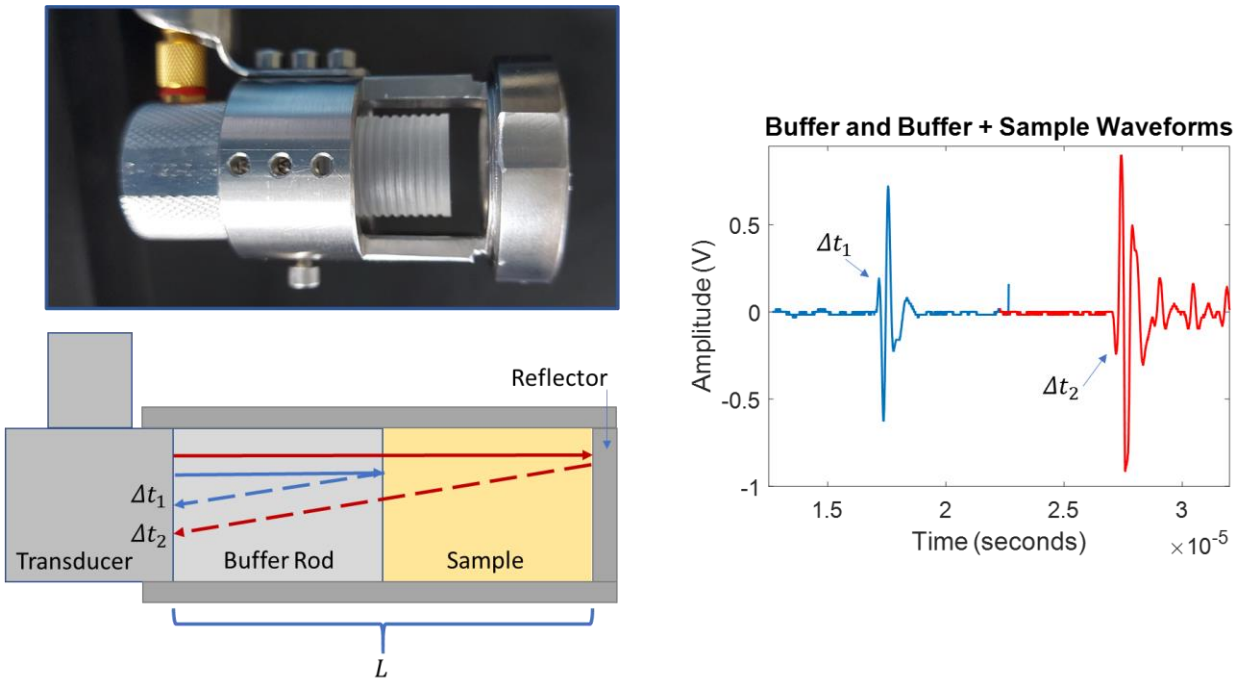

620

621 Figure 2. Schematic drawing of the custom acoustic probe (left) and the measured waveforms
622 obtained by the reflection of the buffer rod (blue), and buffer rod and sample (red) (right). Δt_1 and
623 Δt_2 represent the time-of-flight of the pulse travelling through the buffer rod and through the buffer
624 rod and sample, respectively.

625

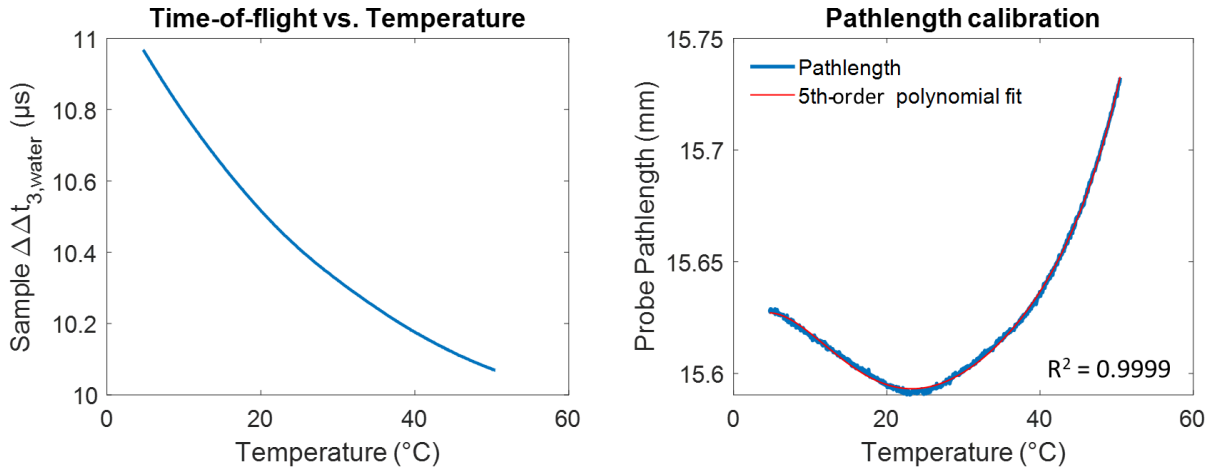

626

627 Figure 3. Measured time-of-flight in distilled water between 60 °C and 5 °C (left), calculated

628 sample path length and 5th-order polynomial fitting (right).

629

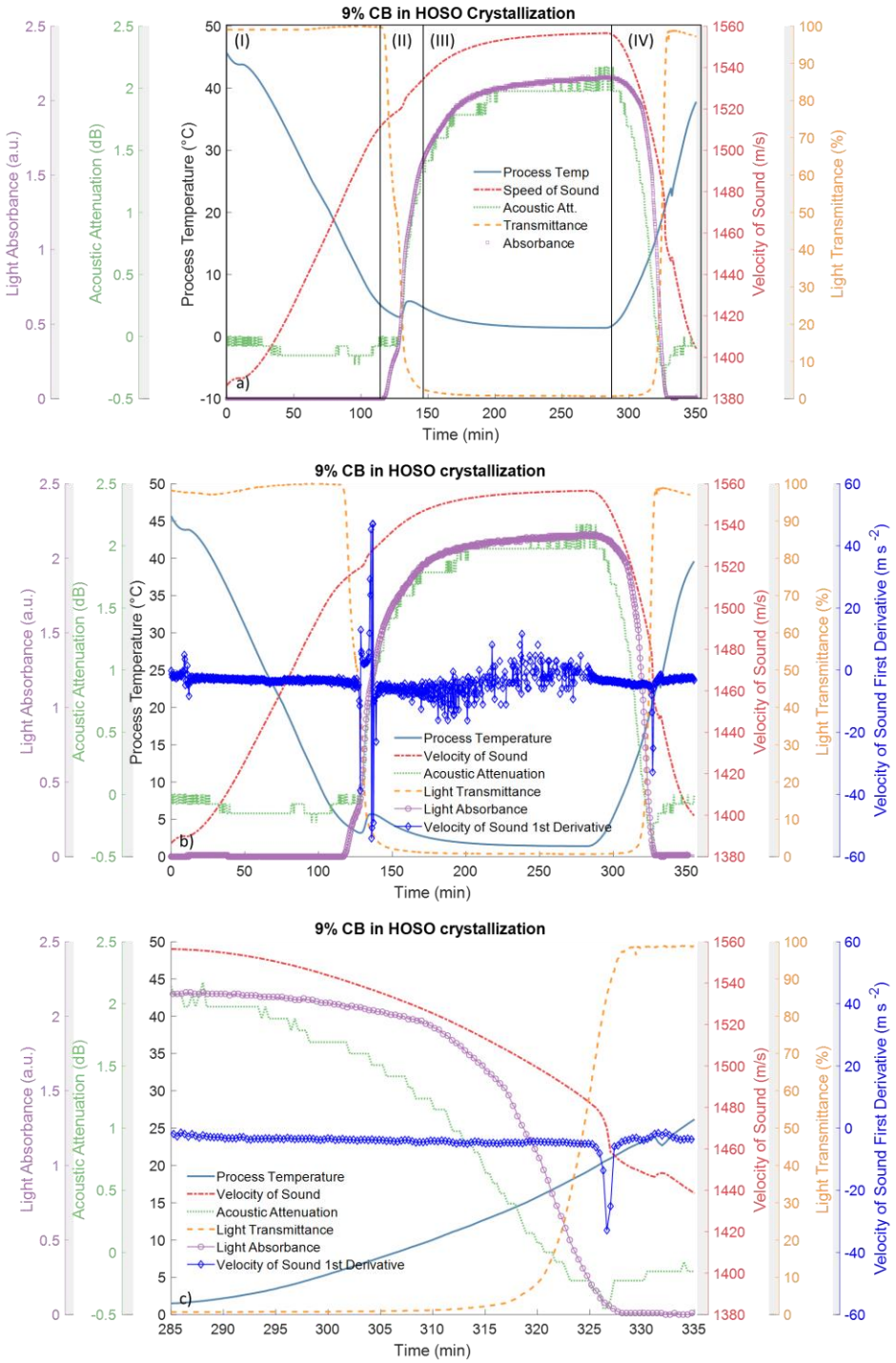

630

631 Figure 4. Process Analytical Technologies (PAT) tools plot of the crystallization of a 9% w/w CB
632 in HOSO blend (a). The different regions of the crystallization process are indicated with roman
633 numerals (I-IV). First derivative plot overlaid on the other PAT tools parameters (b) and

634 enlargement of the melting zone (c). Process temperature (-), velocity of sound (-·-), acoustic
635 attenuation (···), light transmittance (--), light absorbance (-o-) and first derivative of the velocity
636 of sound (-◊-) .

637

638 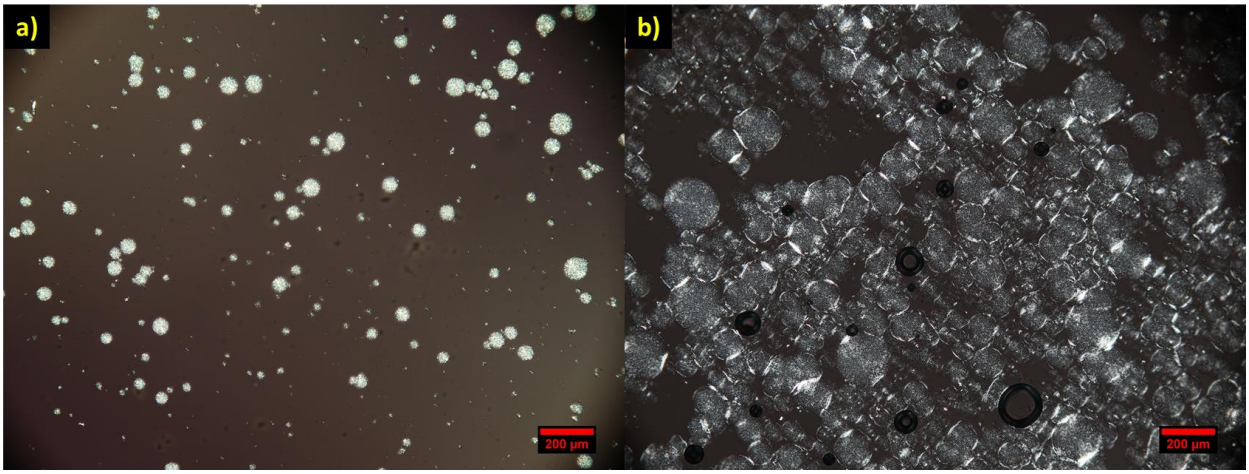

639 Figure 5. Polarized Light Microscopy (PLM) image of a 15% CB in HOSO mixture while
640 crystallizing under shear. Onset of nucleation (a) and formation of the spherical aggregates
641 network (b). Scale bar is 200 µm for both figures.

642

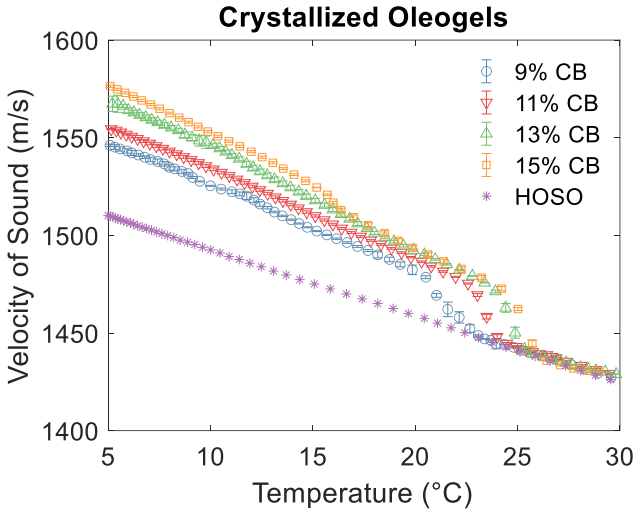

643

644 Figure 6. Velocity of sound of crystallized CB/HOSO oleogels between 5 and 35 °C. The error
645 bars show the standard deviation of three measurements for each concentration. The velocity of
646 sound of the pure HOSO phase is also plotted for reference.

647

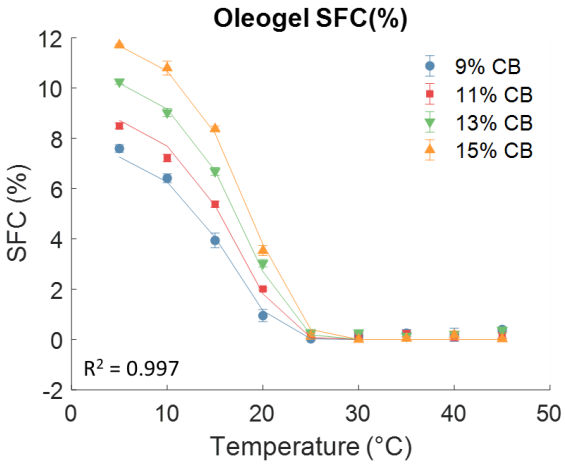

Figure 7. SFC% calculated with *p*NMR with respect to temperature for the different CB/HOSO blends. The datapoints were fitted using a Gompertz-type model, similar to the one described in Farmani (2015).

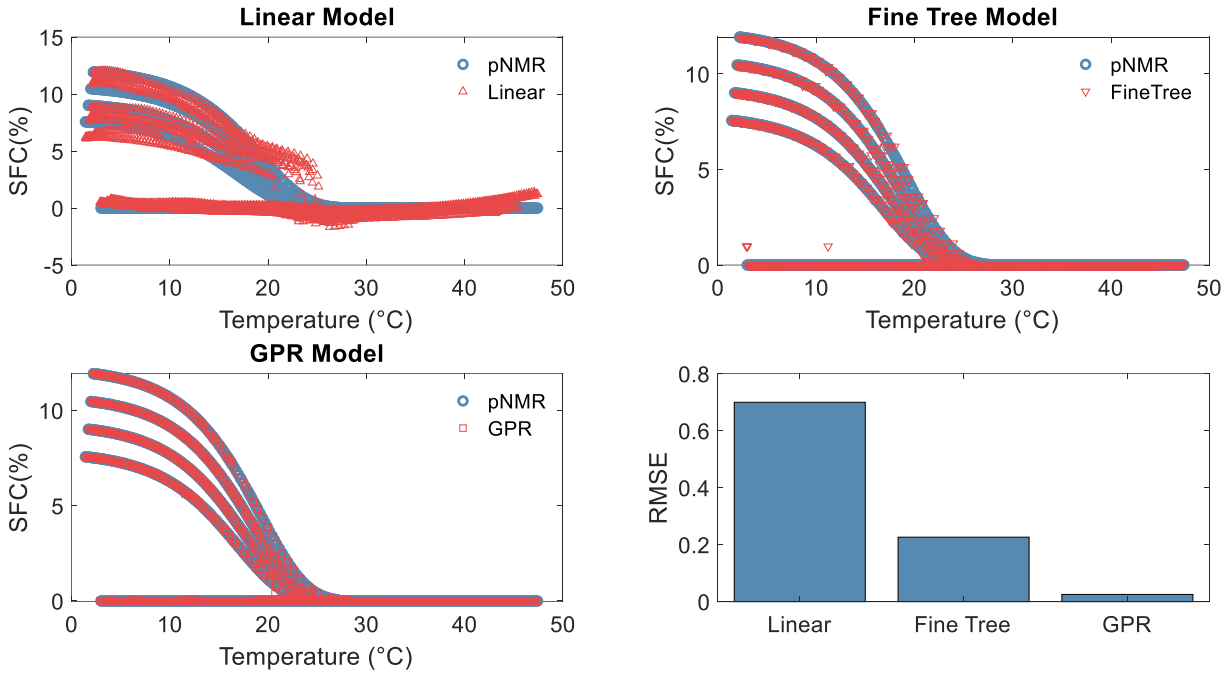

653

654 Figure 8. Predicted SFC(%) values obtained from the supervised-machine learning models,
655 compared against the measured *SFC(%)* from *p*NMR (blue circles) as a function of temperature:
656 a) Linear model (red upward triangles), b) Fine Tree model (red downward triangles), c) Gaussian
657 Process Regression (red squares) and d) histogram plot showing the RMSE on the $SFC(\%)$ values
658 for each model.

659

660

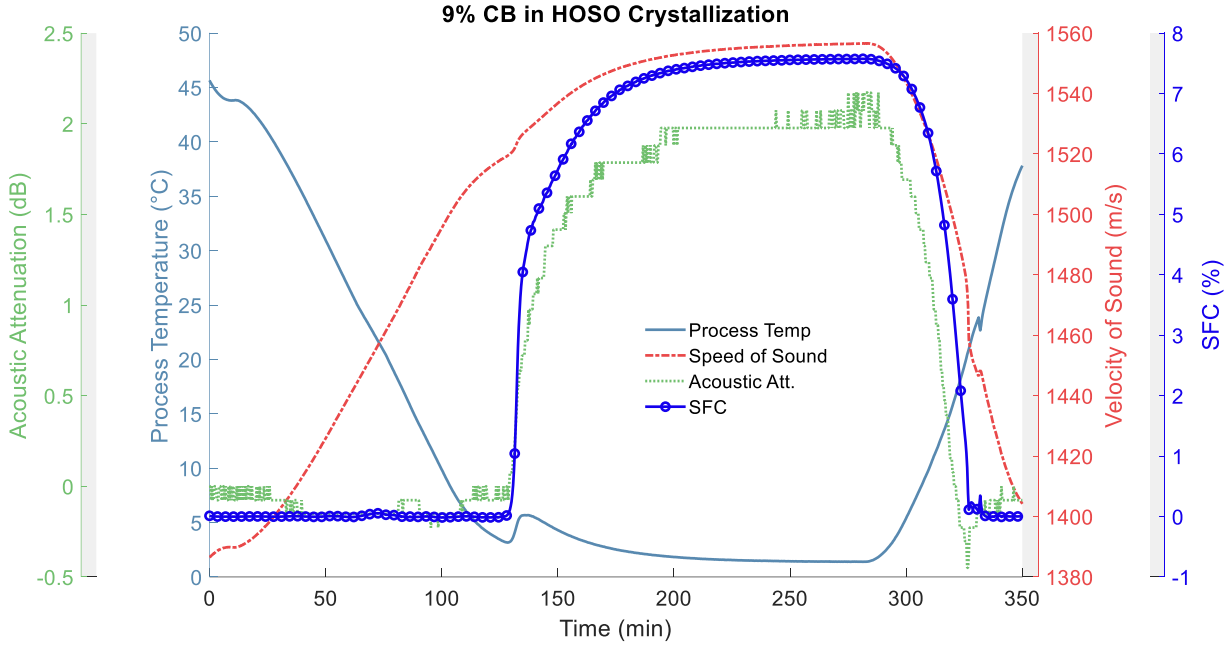

661

662 Figure 9. Process Analytical Technologies (PAT) tools plot of the crystallization of a 9% w/w CB

663 in HOSO blend. Process temperature (-), velocity of sound (-·-), acoustic attenuation (···), and

664 predicted SFC% with the GPR model (-o-).

665

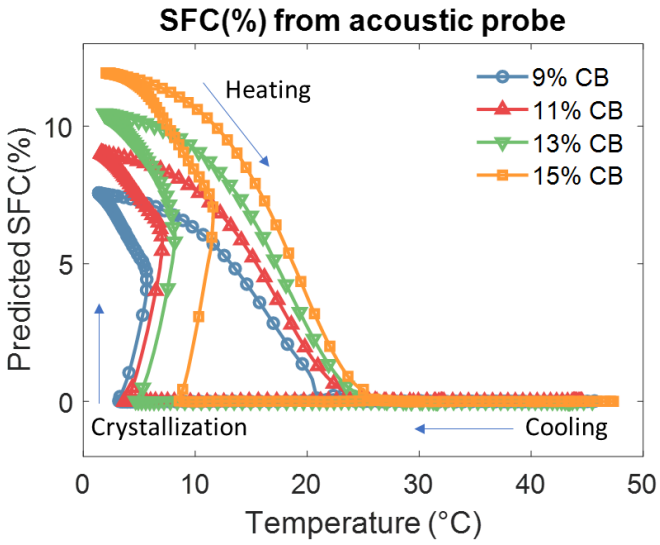

666

667 Figure 10**.** Evolution of ultrasound predicted SFC% during cooling from 40 °C to 5 °C and heating

668 (5 °C to 40 °C) for oleogels containing different CB w/w %.

669

670

671 Table 1. Velocity of sound and acoustic attenuation for oleogel samples at the end of the
672 crystallization (5 °C).

CB % (w/w)	Velocity of Sound (5 °C) (m/s)	Acoustic Attenuation (5 °C) (dB)
9	1545.8 ± 2.2	2.25 ± 1.13
11	1555.1 ± 1.2	2.42 ± 0.09
13	1567.5 ± 6.5	2.61 ± 0.06
15	1578.6 ± 4.0	3.31 ± 0.42

673

674